LRP 759/03 April 2003

Papers presented at the 16th International Symposium on Plasma Chemistry (ISPC-16)

Taormina, Italy, 22 – 27 June 2003

ISSN 0458-5895

Table of contents

Paper ISPC-023 presented at Intl. Symp. Plasma Chemistry, ISPC16, June 22-27, 2003 Taormina, Italy.

Consequences of non-uniform RF plasma potential in large-area capacitive reactors

J. Ballutaud[1], Ch. Hollenstein[1], A.A. Howling[1], L. Sansonnens[1], H. Schmidt[1] and J.P.M. Schmitt[2]

[1] *Centre de Recherches en Physique des Plasmas, Ecole Polytechnique Fédérale de Lausanne, Switzerland*
[2] *Unaxis-France SA, Displays Division, 5 Rue Léon Blum, F-91120 Palaiseau, France*

Abstract
It is conventionally assumed that the plasma potential is the same everywhere in the plasma bulk. However, the non-zero plasma resistivity means that this is not true for the RF plasma potential in large area reactors. The spatial variation in plasma potential due to asymmetric electrode areas is described in terms of a telegraph equation, and the predictions of the model are compared with measurements using electrical probes mounted in the ground electrode of two large area RF plasma reactors.

1. Introduction

In small area capacitive reactors, the RF and DC components of the plasma potential can be assumed to be uniform over all the plasma bulk. In large area reactors, however, the RF plasma potential can vary over a long range across the reactor due to the finite plasma conductivity. A perturbation in RF plasma potential, due to electrode edge asymmetry or the boundary of a dielectric substrate, propagates along the resistive plasma between capacitive sheaths. This study consists of theoretical and experimental sections. In the first part, we develop a model based on a telegraph equation to show how the plasma potential is affected in large area reactors. Perturbations in potentials and currents due to the edge effects of the electrodes will be demonstrated by means of a simple analytical model assuming sinusoidal plasma potential and Langmuir-Hertz sheaths. In the second part we present measurements of the DC current and potential using an array of Langmuir probes in the ground electrode of two large area reactors, one cylindrical and the other rectangular. These measurements are used to test some predictions of the telegraph model.

2. The telegraph equation applied to large area reactors

At the edge of the RF plasma reactor represented in Fig. 1, the electrode areas are asymmetric because of the sidewall. In order to preserve RF current continuity, the RF sheath voltage at the larger area electrode will locally be less than the RF sheath voltage at the smaller electrode, the sum of the potentials being equal to the applied RF voltage. In the middle of the reactor, however, the electrode areas are symmetric and both RF sheath voltages would be expected to equal half of the RF voltage V_{RF}. The different sheath potentials in these two zones can be reconciled by allowing the RF plasma potential to vary across the reactor with a characteristic damping length Λ due to the non-zero plasma resistivity [1]. The redistribution of the sidewall RF current is represented by a lateral RF current in the simplified 1D equivalent circuit model in Fig. 1.
In the presence of a perturbation $\underline{V}(x,t)$ due to the sidewall, the ground sheath RF potential is

$$\underline{\tilde{U}}(x,t) = \frac{V_{RF}}{2} \cdot e^{i\omega t} + \underline{V}(x,t).$$

A lateral current $\underline{I}(x,t)$ flows through R and L, the plasma resistance and inductance per unit length, where

$\frac{\partial \underline{V}}{\partial x} = -R\underline{I} - L\frac{\partial \underline{I}}{\partial t}$, and

$\frac{\partial \underline{I}}{\partial x} = -C\frac{\partial \underline{V}}{\partial t}$, where C is the combined sheath parallel capacitance per unit length. We therefore obtain

$\frac{\partial^2 \underline{V}}{\partial x^2} = LC\frac{\partial^2 \underline{V}}{\partial t^2} + RC\frac{\partial \underline{V}}{\partial t}$ which is the telegraph equation.

The damping term dominates if $R/\omega L = \nu_m/\omega >> 1$ (high pressure, low excitation frequency).

In 1D Cartesian coordinates, with $\underline{V}(x,t) = \underline{V}(x)e^{i\omega t}$, the particular solution is

$$\underline{V}(x,t) = \underline{B}\exp\left(\frac{\pm x}{\underline{\Lambda}}\right)e^{i\omega t} = \underline{B}e^{\pm x/\Lambda}e^{i(\omega t \pm x/\Lambda)} \text{ where } \underline{\Lambda} = \frac{\Lambda}{(1+j)} \text{ and } \Lambda = \sqrt{\frac{2}{\omega RC}} = \omega_{pe}\sqrt{\frac{ag}{\omega\nu_m}}$$

with a the sheath width, g the plasma bulk height, ν_m the electron-neutral collision frequency, and ω_{pe} the electron plasma frequency. The voltage perturbation is a strongly-damped wave; the value of Λ increases with electron density, sheath thickness and bulk plasma height, and decreases with higher excitation frequency and collision frequency (higher pressure). If inductance is included, the damping length increases and the wavelength decreases. The boundary condition at the sidewall is

$\left.\frac{\partial \underline{\tilde{U}}}{\partial x}\right|_{x=L} = -I_{sidewall} R = -\underline{\tilde{U}}(L) j\omega C_W R$ where C_W is the sheath capacitance at the sidewall.

Note that this simple model assumes the plasma to be a uniform slab. The RF plasma potential is the same as the ground sheath RF voltage in this simple model where the impedance of the bulk plasma is neglected compared to the sheath impedance. The combination of a reduced and augmented sheath potential at the asymmetric edge results in a net increased power deposition at the edge. Comparison between this solution and solution of Maxwell's equations for the voltage distribution in a lossy dielectric shows that the telegraph model is a good approximation.

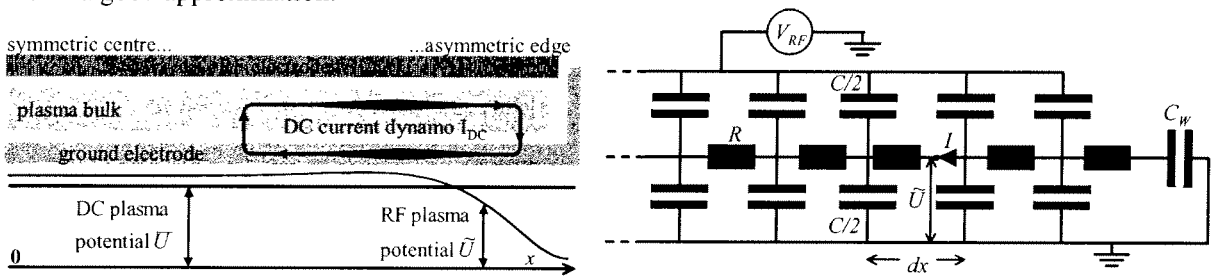

Figure 1. Left: schematic cross-section of an asymmetric reactor, from the centre to the right hand sidewall, showing profiles of the RF and DC components of the plasma potential, and the 'dynamo' of DC current between the ground electrode and the plasma. Right: the equivalent circuit used for the telegraph description. The sidewall sheath capacitance is represented by C_W.

3. Consequences of non-uniform RF plasma potential

Since the DC plasma potential is uniform across the plasma, and a conducting electrode is an equipotential surface (in absence of a dielectric substrate), a consequence of the non-uniform RF plasma potential is that local ambipolarity cannot be satisfied over all the electrode surface. This is because the RF and DC sheath voltages, $\tilde{U}$ and $\overline{U}$ respectively, cannot everywhere simultaneously satisfy the self-rectification condition [2] for zero DC current flow, which is $\overline{U} = \frac{T_e}{2}\ln\left(\frac{M_i}{2.3m_e}\right) + T_e \ln\left[I_o\left(\frac{\tilde{U}}{T_e}\right)\right]$ (a sinusoidal plasma potential, and therefore sinusoidal sheath voltages, have been assumed for the sake of convenience in this simplified model). Any spatial variation in the plasma RF potential will necessarily lead to time-averaged current flow across the sheaths. However, the reactor is capacitively coupled which prevents any DC current in the external circuit. Therefore, any DC current which flows across the sheaths must circulate through the plasma and return via the conducting surface of the electrode, so that the integral of the DC current over the electrode area is zero. The DC plasma potential adjusts to satisfy this condition at the ground electrode, and the self-bias of the RF electrode adjusts to satisfy this condition at the RF electrode. Consequently, the reactor asymmetry drives DC current 'dynamos' within the reactor as shown in Fig. 1. These DC sheath currents can be measured with grounded probes in the ground electrode surface, as shown in the following sections. These probes measure the local DC current density $j(\underline{x})$ to the ground electrode. The DC floating potential of the surface probes can also be used to give an indirect indication of the spatial variation of the plasma RF potential amplitude: in the previous equation, where the plasma potential is not equal to the value necessary for local ambipolarity, a floating probe in the electrode surface will have the time-averaged voltage:

$\overline{V}_f(\underline{x}) = \overline{U} - T_e \ln\left[I_o\left(\frac{\tilde{U}(\underline{x})}{T_e}\right)\right] - \frac{T_e}{2}\ln\left(\frac{M_i}{2.3m_e}\right) \neq 0$ because the grounded surface is not floating.

In the limit $\tilde{U}(\underline{x}) >> T_e$: $\overline{V}_f(\underline{x}) \approx \overline{U} - \tilde{U}(\underline{x}) + \frac{T_e}{2}\ln\left(2\pi\frac{\tilde{U}(\underline{x})}{T_e}\right) - \frac{T_e}{2}\ln\left(\frac{M_i}{2.3m_e}\right)$, therefore $\Delta\overline{V}_f(\underline{x}) \approx -\Delta\tilde{U}(\underline{x})$.

i.e. the negative of the ground electrode probe floating potential $\overline{V}_f(\underline{x})$ is approximately equal to the variation in plasma potential amplitude $\tilde{U}(\underline{x})$ across the reactor. To summarise: the experimental measurements in this work are made with probes mounted in the ground electrode. The current to a grounded probe represents the DC current density flowing to ground; and the negative of the probe floating potential represents approximately the deviation of the RF plasma potential amplitude from the value necessary for local ambipolarity.

4. Experimental results and comparison with a telegraph model in a cylindrical reactor

Figure 2 shows the measured radial profiles, across the one metre diameter of a cylindrical reactor, of the optical emission intensity, the DC current density, and the probe floating potential (the probes were mounted in the surface of the ground electrode). In this reactor, the grounded sidewall (1 cm high) is smaller than the sidewall of the RF electrode (2 cm high), therefore the grounded electrode has the smallest area, opposite to the case shown in Fig. 1. These radial profiles were cylindrically symmetric, as shown in the figure, provided that the sidewall height was precisely the same around the reactor circumference.

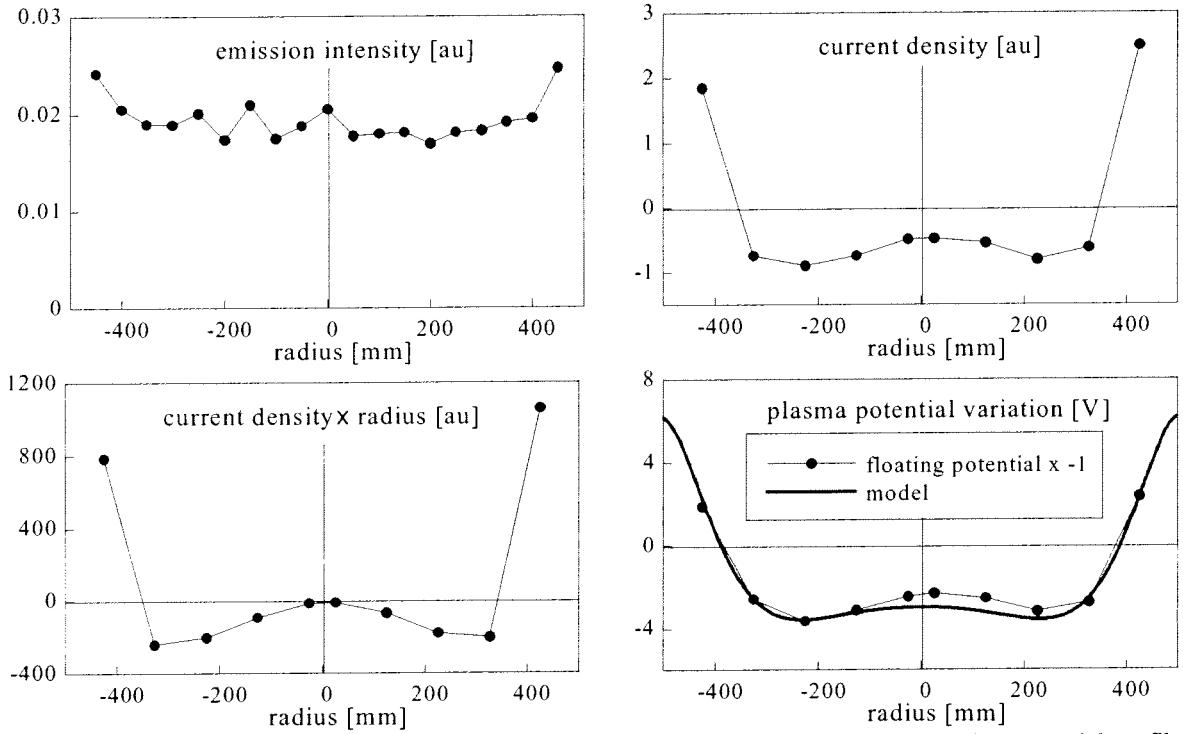

Figure 2: Measured profiles of emission intensity, DC current density, DC current, and floating potential profiles for probes mounted along a 1 m diameter of the cylindrical reactor. The DC current balance is approximately satisfied; and a comparison of the deduced RF plasma potential amplitude profile with a numerical solution of the telegraph equation (Λ=0.06 m) is also shown. Electrode gap 3 cm, grounded sidewall 1 cm high, RF sidewall 2 cm. Plasma parameters: argon/hydrogen flow ratio 2:1, 13.56 MHz, pressure 100 mTorr, 200 W RF power.

The damping length Λ is estimated to be a few cm [1] for the plasma parameters given in the caption to Fig. 2. At 13.56 MHz, any standing wave non-uniformity is negligible since the RF wavelength is much larger than the machine. The edge plasma non-uniformity can be seen on the emission intensity profile. The plasma power is higher towards the reactor edge, in agreement with the telegraph model. The radial profiles of the DC current density and floating potential are both bipolar, with the zero crossing point at the same radius as expected. This radius is the null point about which the DC dynamo rotates from larger to smaller radii. DC current from probe to plasma is defined as positive throughout this work. The surface integral $2\pi \int_0^R j(r)\,dr$ of the current density $j(r)$ shows that the net DC current to the ground electrode is indeed zero (within experimental error due to the limited number of probes defining the DC current profile) as expected for the capacitively-coupled reactor. The DC current density near the wall is majority electron current, being

balanced by a majority ion current within the radius of zero current; this corresponds to the current flow in Fig. 1 for the smaller (upper) electrode.

The negative profile of the probe DC floating potential is compared with a numerical solution of the telegraph equation for the RF plasma potential amplitude in cylindrical geometry. Given the approximations made and the assumption of uniform plasma resistivity and sheath capacitance in the telegraph model, there is reasonable agreement for a value of Λ = 0.06 m. Note that the deduced envelope of the RF plasma potential amplitude increases towards the wall, which corresponds to Fig. 1 for the smaller (upper) electrode.

When the sidewall height asymmetry was reversed (grounded sidewall larger than the RF electrode sidewall), the DC current and floating potential profiles were inversed, as expected. If the sidewall height differed by a few mm around the perimeter, the cylindrical symmetry was broken and the profiles became skewed with a marked slope across the diameter, demonstrating that the sidewall geometry can have a strong influence on the plasma uniformity, even across the entire 1 m diameter. However, when the RF and grounded sidewalls were accurately equalised (equal effective sidewall areas for the ground and RF electrodes), then the measured values of probe current density and floating potential were strongly reduced along the whole diameter, indicating that there was no systematic variation in RF plasma potential, and the plasma emission intensity was uniform. Any remaining edge non-uniformity is due to fringing fields which are localized close to the junction between the sidewalls.

As a supplementary demonstration of the experimental method, it is interesting to consider measurements performed at a higher RF frequency where standing wave effects become important, and even dominate edge effects. Figure 3 shows the same profile measurements as for Fig. 2, but at 67.8 MHz. In contrast to a telegraph model at low frequency, the plasma profile is dominated by a central peak. The RF voltage amplitude has the Bessel function radial distribution $J_o(k_{eff}r)$, where k_{eff} is the effective wavenumber due to the plasma permittivity [1]. This voltage profile is a solution of Maxwell's equations in parallel plate cylindrical geometry, and is independent of plasma resistivity effects. Nevertheless, any phenomenon which causes the RF plasma potential to be non-uniform (in the presence of a uniform DC plasma potential) will cause DC currents to circulate for the same reasons as given in the previous section. Figure 3 shows that the current density profile, as measured by the grounded probes, integrates approximately to zero. Furthermore, the negative floating potential profile approximates to a Bessel profile, shifted by a DC value corresponding to the DC plasma potential. This shows the probe method used in a different context independently of the telegraph effect.

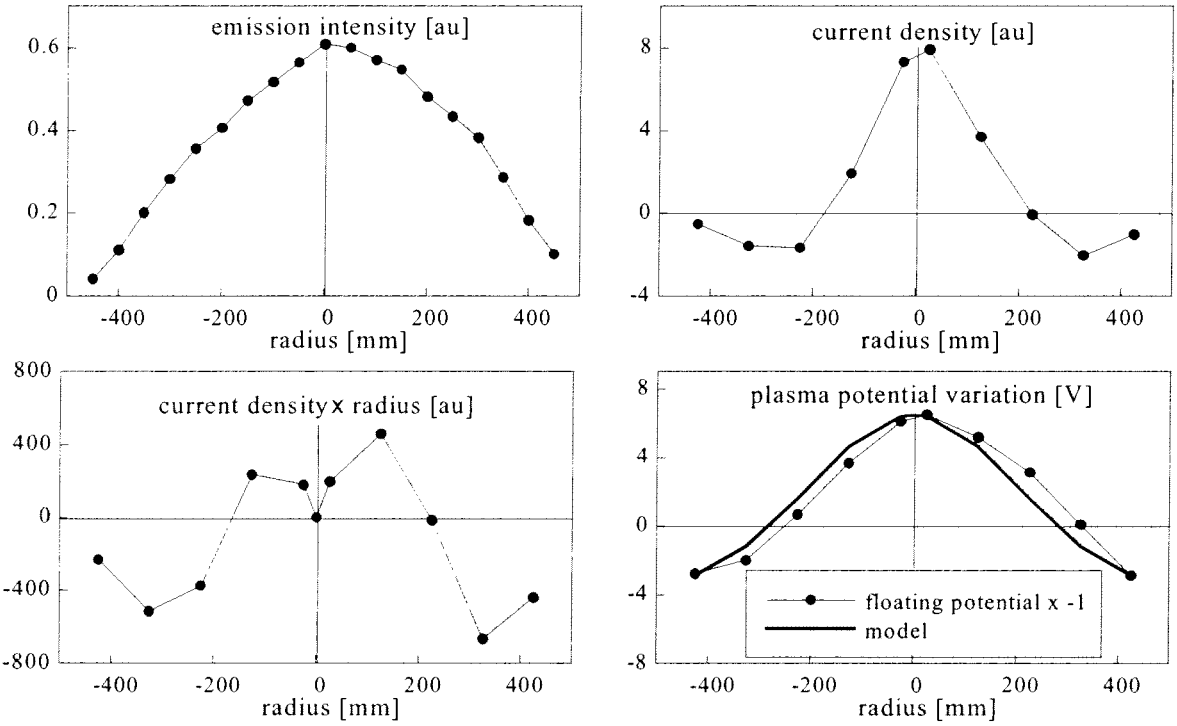

Figure 3: The same cylindrical reactor as for Fig. 2, but at 67.8 MHz, Ar 250 mTorr, 300 W. The RF plasma potential amplitude profile, deduced from the probe floating potential profile, is compared with a Bessel function solution for the standing wave. The standing wave effect is seen to dominate the edge asymmetry effect at this high frequency.

5. Experimental results and comparison with a telegraph model in a rectangular reactor

The rectangular reactor has electrode dimensions 47 cm by 57 cm, with a grounded sidewall of height 2.5 cm. The grounded electrode now has the largest area, corresponding to Fig. 1, which is the opposite case to the cylindrical reactor in the previous section. An array of surface probes is mounted in the ground electrode along a line from the reactor axis towards the sidewall (see Fig. 5 for the probe positions) with another probe in the sidewall itself. In Fig. 4(a) we see that the sign of the current density is inversed (with majority DC electron current contribution this time on the interior of the grounded electrode surface) with respect to Fig. 2 because the electrode area asymmetry is reversed. In contrast to the data presented up to now with no substrate, Fig. 4(c) shows the DC current density measurement in presence of a centrally-positioned glass substrate 37 cm x 47 cm, leaving a 5 cm gap between the substrate edge and the sidewall. The insulating substrate now constrains the DC current dynamo to circulate in the 5 cm gap between the sidewall and the substrate. The DC plasma potential and the RF electrode self-bias voltage adjust to maintain global ambipolarity. The integral of the DC current $\int_0^L j(x)\,dx$ is still roughly zero although accurate values are difficult to obtain because the current density in the vicinity of the sidewall is not measured with sufficient spatial resolution.

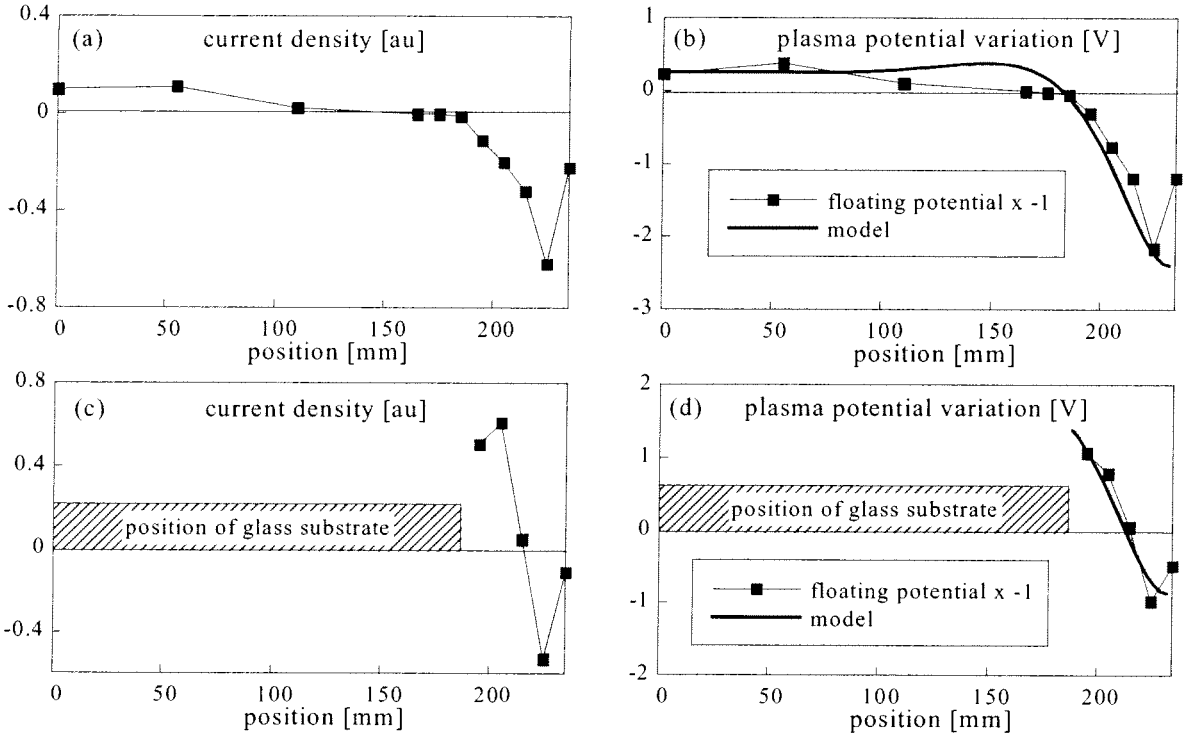

Figure 4: Measured DC current density and DC floating potential profiles for probes mounted along the 0.235 m halfwidth of a rectangular reactor. Top: no substrate. Bottom: with a glass substrate to 5 cm from the sidewall. The DC current balance is approximately satisfied in both cases; and comparisons of the deduced RF plasma potential amplitude profile with a telegraph solution (Λ=0.02 m) are also shown. Hydrogen plasma parameters: 40.7 MHz, 0.6 mbar, 60 W.

The envelope of the RF plasma potential, inferred from the negative of the DC floating potential profile, decreases towards the wall, also opposite to the behaviour for the previous results in Fig. 2 for the same reason of reversed electrode area asymmetry. This fall-off in amplitude is to reduce the RF current contribution from the grounded sidewall. The negative profile of the probe DC floating potential is compared with the analytic expression for the RF plasma potential amplitude in Cartesian geometry. There is reasonable agreement between the measurement and the telegraph 1D profile using a damping length distance Λ = 0.02 m, provided that the sidewall current is 2-3 x smaller than the extrapolated value, as observed experimentally. It seems reasonable that this is due to imperfect contact of the plasma with the sidewall. It is interesting to note that the condition for local ambipolarity above a thin insulating substrate can cause its surface potential to be maintained at a negative value – this would be impossible if the plasma potential were unique. The consequent negative charging of a hot glass substrate has been measured in many

different conditions [3], and is supporting evidence for the telegraph effect. The DC sheath potential then varies over a dielectric substrate resulting in a non-uniform ion bombardment energy.
The experimental parameters were purposely chosen to obtain a damping length much smaller than the reactor width, because otherwise a one-dimensional treatment is not justified. Fig. 5 shows 2D solutions of the telegraph equation in the reactor geometry for Λ = 0.03 m and 0.1 m. For Λ = 0.1 m, the voltage perturbation extends over a large distance, and the enhanced area asymmetry due to the corner sidewalls influences the DC current dynamo flow far from the corners, to the extent that all the probes measure a positive DC current density (unipolar profile), as observed, and the negative DC current density is concentrated in the corners. For Λ = 0.03 m and less, the range of influence of the corners is restricted, and, for most of the reactor perimeter, the perturbation can be described by the 1D model as used in Fig. 4.

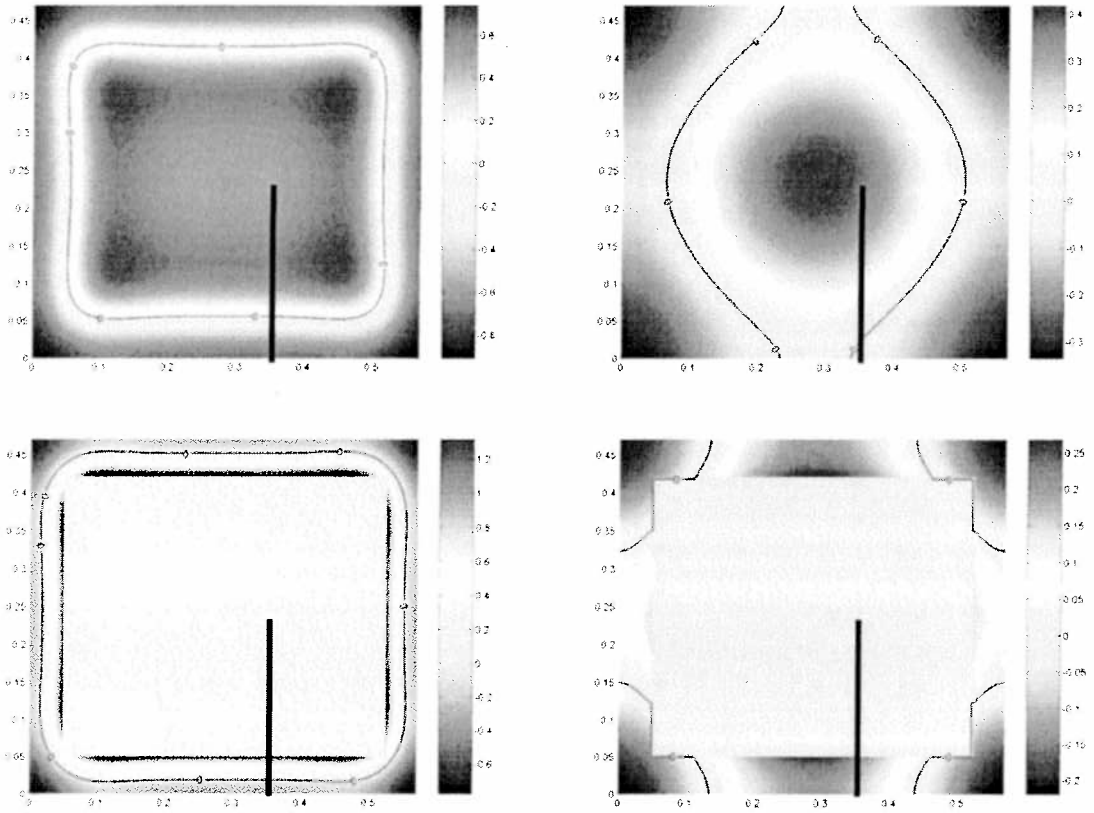

Figure 5: 2D colour contour plots of the RF current density solutions of the telegraph equation for damping lengths Λ = 0.03 m (left) and 0.1 m (right). Above: no substrate; below: with glass substrate. The location of the probe array is shown by the bar. The contour of zero DC current is indicated. For Λ = 0.03 m, the 1D description along the halfwidth at the probe positions is a good approximation. For Λ = 0.1 m, the current density everywhere is strongly influenced by the corner sidewalls.

6. Conclusions

Model and measurements with surface probes show that non-symmetric electrode areas cause a spatial variation in the RF plasma potential which can be described by a telegraph equation. This leads to non-uniform RF sheath voltages and RF power density. The non-uniform RF plasma potential in presence of the uniform DC plasma potential results in non-ambipolar currents circulating through the plasma and along conducting surfaces. If the electrode sidewall areas are accurately equalized, then the RF plasma potential amplitude and the power density are uniformalised.

References

[1] J. Schmitt, M. Elyaakoubi and L. Sansonnens – Plasma Sources Sci. Technol. **11**, A206 (2002).
[2] K.-U. Riemann – J. Appl. Phys. **65**, 999 (1989).
[3] A.A. Howling, A. Belinger, P. Bulkin, L. Delaunay, M. Elyaakoubi, Ch. Hollenstein, J. Perrin, L. Sansonnens, J. Schmitt and E. Turlot – 15th Int. Symp. Pl. Chem. July 9–13 (2001) Vol. I pp33-39.

Presented at the 16th International Symposium on Plasma Chemistry (ISPC-16)
Taormina, Italy, 22 – 27 June 2003

A novel approach to interpret enthalpy probe measurements in low pressure supersonic plasma jets

J.-L. Dorier[1], B. Jodoin[2], M. Gindrat[1], A. Blais[2], C. Hollenstein[1], and G. Barbezat[3]

[1] *Plasma Physics Research Centre, Swiss Federal Institute of Technology, Lausanne, Switzerland*
[2] *Department of Mechanical Engineering, University of Ottawa, Ottawa, Canada*
[3] *Sulzer Metco Switzerland AG, Wohlen, Switzerland*

Abstract

The first steps in the development of a new method to interpret enthalpy probe measurements in supersonic plasma jets is presented. This method relies on a special post-shock probe which allows measurement of the (unknown) static pressure downstream of the shock induced by the probe. Conservation equations are used to infer the jet parameters in two steps: backwards from stagnation to post-shock, and then to free stream. The assumptions of this new method are less restrictive than previous ones. The new method will also allow for inclusion of non-LTE effects. Comparison with previous approaches shows the improved accuracy of the described technique.

1. Introduction

Low Pressure Plasma Spraying (LPPS) processes, using plasma torches operated at reduced pressure, have emerged as reliable technologies with broad industrial successes for the deposition of numerous coatings [1]. However, the majority of advances in LPPS have been made by empirical means and have reached their limit [2]. To further improve the control and quality of the processes, and to develop new applications, a more quantitative approach is required in which the fundamental physics of the process should be investigated. In particular, the phenomena controlling the expanding plasma jet should be studied both experimentally and by numerical simulations. This requires the knowledge of key parameters such as the temperature, pressure, chemical composition, velocity or local heat flux.
To measure these parameters, the enthalpy probe measurement technique has been extensively applied in Atmospheric Plasma Spraying (APS) jets assuming Local Thermodynamic Equilibrium (LTE) and incompressible flow [3]. However, the latter is not valid in low-pressure plasma jets and the formation of a normal shock wave (NSW) in front of the probe must be accounted for. Although specific technological constraints (low gas density) have been recently overcome [4], there are still severe conceptual complications in the use of enthalpy probes for low-pressure plasma jets.
First, the Pitot tube technique commonly used for the determination of the flow velocity cannot be directly applied because these jets are usually not in aerodynamic equilibrium with the surrounding atmosphere [5]. This means that the free stream local static pressure (P_1) can differ strongly from the chamber pressure. Erroneous results are obtained if the latter is used to approximate P_1 [4, 6], which is not directly accessible by measurement. A second complication comes from the required assumptions about the stagnation process that have been made in order to infer the free-stream jet properties from the quantities measured downstream of the shock [7]. Third, the low collisionality and high velocity of these flows can lead to deviations from LTE, which cannot be accounted for with the usual approaches [4, 6, 7].
In a previous attempt to solve the aerodynamic non-equilibrium problem, P_1 has been determined from numerical simulations of the plasma flow, which were then back-validated by the enthalpy probe results [8]. This approach, although valid, is complex and inconvenient to use.
The new enthalpy probe measurement approach presented here improves the accuracy of the technique by introducing a new way to deal with and interpret the data provided by the probe. It does not require the knowledge of the jet static pressure P_1, which is a major advantage over existing methods. It is also less restrictive in the assumptions used and can be modified to include non-LTE effects. As before, the stagnation pressure and enthalpy (P_{02} and h_{02}) behind the NSW induced by the probe are measured and used to compute the flow properties of the free plasma jet in front of the NSW (P_1, T_1, M_1, V_1). To achieve that, the jet static pressure behind the NSW (P_2) is required and a special post-shock static pressure probe (PSSPP) is developed and used as presented in the next section.

The experimental technique is described in section 3. In section 4, our new approach is demonstrated for the interpretation of enthalpy probe measurements performed on an argon plasma jet at 10 mbar. These results are discussed and compared with those obtained by previous approaches [4, 6 - 8].

2. Description of the method

The deceleration of the free supersonic plasma jet towards the enthalpy probe can be seen as two separate evolutions (figure 1). The first evolution, from state (1) to state (2), represents the strong deceleration from the free stream conditions (1) to the post-shock conditions (2) through the NSW present in front of the enthalpy probe. The second evolution, from state (2) to state (02), represents the deceleration of the flow after the NSW to the stagnation condition in the probe. The proposed method consists of solving the governing flow equations for the two evolutions, starting backward from (02) to (2) and then from (2) to (1). The required data are obtained from the enthalpy probe (P_{02} *and* h_{02}) and the post-shock static pressure probe (P_2) described below.

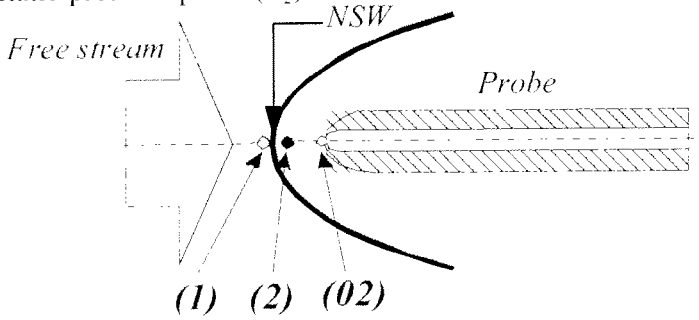

Figure 1 : Schematic representation of the free plasma jet deceleration by the probe.

Evolution (02) to (2)

Knowing from the enthalpy probe P_{02} and h_{02} and assuming that at stagnation the plasma is in local thermodynamic equilibrium (LTE), it is possible to find the plasma stagnation composition (ω_{Ar02}, ω_{Ar+02}, ω_{e02}), temperature (T_{02}) and entropy (s_{02}). Assuming that the flow is steady and reversible, the mass and energy conservation can be combined to give:

$$h_{02} = h_2 + \frac{V_2^2}{2}$$

In the same way the mass conservation and the second law can be combined to give:

$$s_{02} = s_2.$$

Assuming that the plasma is in LTE at location (2), and since s_2 (from the second law) and P_2 (from the post-shock static probe) are known, it is possible to find the plasma composition (ω_{ar2}, ω_{ar+2}, ω_{e2}), temperature (T_2) and enthalpy (h_2) behind the NSW [9, 10]. Using the energy equation, one can then find the velocity (V_2) behind the NSW. The flow properties are then all known at location (2).

Evolution (2) to (1)

The fundamental governing laws are again applied for this evolution and are expressed as:

$$\rho_1 V_1 = \rho_2 V_2 \quad \text{(mass conservation)}$$

$$p_1 + \rho_1 V_1^2 = p_2 + \rho_2 V_2^2 \quad \text{(momentum conservation)}$$

$$h_1 + \frac{V_1^2}{2} = h_2 + \frac{V_2^2}{2} \quad \text{(energy conservation)}$$

$$s_2 > s_1 \quad \text{(2nd law of Thermodynamics)}$$

This system of equation is closed with a state equation, $s=s(P,T)$. Due to strong non-linearity, a graphical Fanno-Rayleigh line solution method [11] was preferred to a classical iterative one. A general representation of the Fanno and Rayleigh lines is presented in figure 2. The Fanno line represents

solutions to the mass, energy and state equations on a Mollier (enthalpy *vs* entropy) diagram. The Rayleigh line represents solutions to the mass, momentum and state equation on the same diagram. The flow going through the NSW must obey all three mass, momentum and energy conservation equations as well as the state equation. Therefore, the solutions ((1) and (2)) of the system must lie on the intersections of the Fanno and the Rayleigh lines.

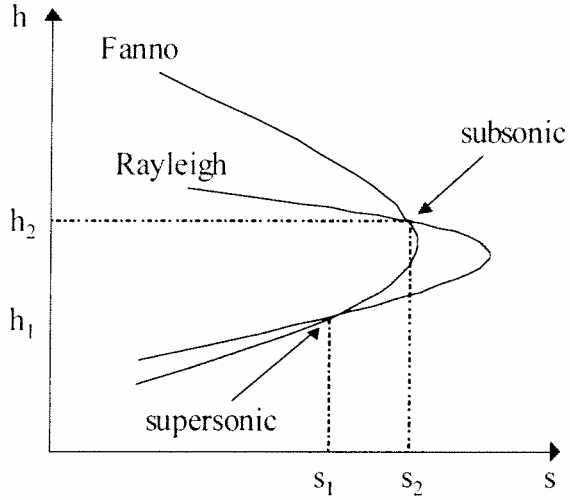

Figure 2 : General representation of the Fanno and Rayleigh lines on a Mollier diagram.

As shown, two (h,s) combinations lie on both lines. To determine which is condition (1) and which is condition (2), the second law of Thermodynamics is used : s_2 should be larger than s_1. Therefore it becomes clear that the intersection of the Fanno and Rayleigh lines at the smallest entropy value represents the flow at location (1). The flow properties at location (1) are then found by reading the Mollier diagram.

3. Experimental

The plasma jet under investigation is produced by a Sulzer Metco F4-VB gun operated in a vacuum chamber. The operation conditions are 40 SLPM of pure argon flow with a 400 A current. For the 10 mbar chamber pressure used here the plasma jet flow is under-expanded, as shown in figure 3. Further details about the experimental set-up and phenomenology of under-expanded plasma flows are described elsewhere [5, 8]. The enthalpy probe system, described in more detail in [4], is a specially designed version [12], which allows measurements down to a pressure of 2 mbar. Two different types of probe tips are used in the present study. The first type is a usual, water-cooled, stainless steel Pitot tube (3.2/0.8 mm external/internal diameter, see Fig. 4a). The second type is a specially designed graphite appendice, the Post-shock static pressure probe (PSSPP), which is plugged in the orifice of a probe (Fig 4b). The first probe allows measurement of the stagnation quantities P_{02} and h_{02}. The second one is equipped with a 0.5 mm diameter static pressure tap that allows measurement of the static pressure behind the NSW (P_2) using the enthalpy probe system (Fig 4c).

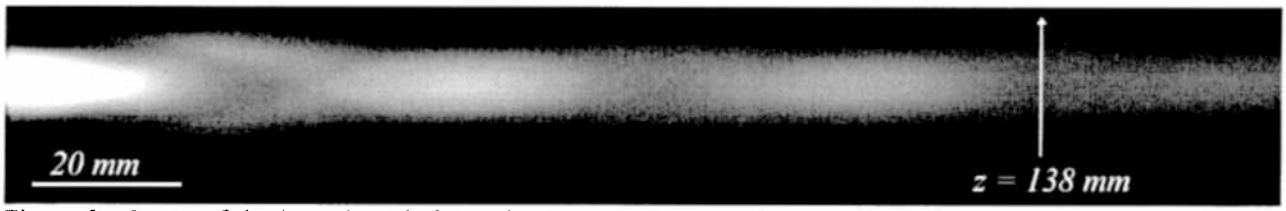

Figure 3 : Image of the investigated plasma jet (400A, 40 SLPM Ar, 10 mbar). "z =138 mm" indicates the axial position of the probe measurements presented below.

The design of the PSSPP is made as follows: First the profile and angle of the graphite probe have been determined in order to insure that the NSW-probe distance and the stagnation pressure are similar to those obtained with the enthalpy probe. This ensures that the PSSPP induces the same shock strength as the enthalpy probe. Second, numerical simulations of the flow around the PSSPP were conducted to get a mapping of the static pressure after the NSW. These simulations show that the static pressure behind the NSW (P_2), is recovered at a given location on the PSSPP surface, due to the flow re-acceleration.

The pressure tap was then tuned to this location, obtained from the numerical simulations. Finally it was checked that P_2 obeys the condition : $0.6\ P_{02} < P_2 < P_{02}$, ensuring that the flow has undergone a NSW [11].

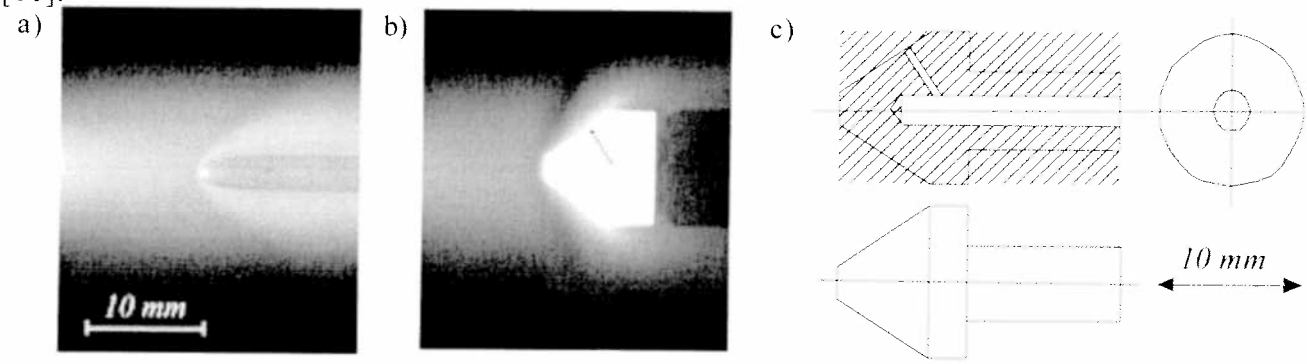

Figure 4 : Images of (a) the enthalpy probe tip and (b) one of the PSSPP developed for the p_2 measurement, both located on jet axis at 138 mm from nozzle exit. (c) shows a drawing of the PSSPP geometry with the pressure tap.

Measurements have been made at different locations in the plasma jet, and tuning of the PSSPP has been made with various shapes and pressure tap positions. The experimental error on the measured pressure is estimated to be within 2% of the measured value. For every measurement location an image of the probes has been acquired with a CCD camera equipped with a band-pass filter to reduce the bright emission from the heated PSSPP in favor of the emission from the plasma jet.

4. Results and discussion

The new approach is tested in the supersonic plasma jet described in the previous section and shown in Figure 3. Measurements are taken at the location z = 138 mm, shown on figure 3, for 5 radial positions, (r = 0, 2, 4 and 8 mm). The choice of this location is justified as follows: It is desired to test the new approach in a zone where the jet is not in aerodynamic equilibrium and where the static pressure changes radially. Such a region would allow testing of the sensitivity of the new probe. By looking at Figure 3, it is possible to deduce that the location z = 138 mm corresponds to the beginning of an expansion zone (where the pressure near the axis of the jet is higher than the chamber pressure) and that it well suits the requirements to test the method. Table 1 presents the raw data (h_{02}, p_{02} and P_2) as measured.

Table 1 : Raw data as measured, used in the new method

r (mm)	h_{o2} (kJ/kg)	p_{o2} (Pa)	p_2 (Pa)
0	9556	5941	3943
2	10982	5905	3731
4	8009	5752	3519
8	3236	4471	3085

The results of the new approach are then compared with the results obtained using the classic approach [4, 6, 7, 8]. Figure 5 presents a comparison of the static pressure (P_1), temperature (T_1) and velocity (V_1) profiles across the plasma jet as computed using both methods.

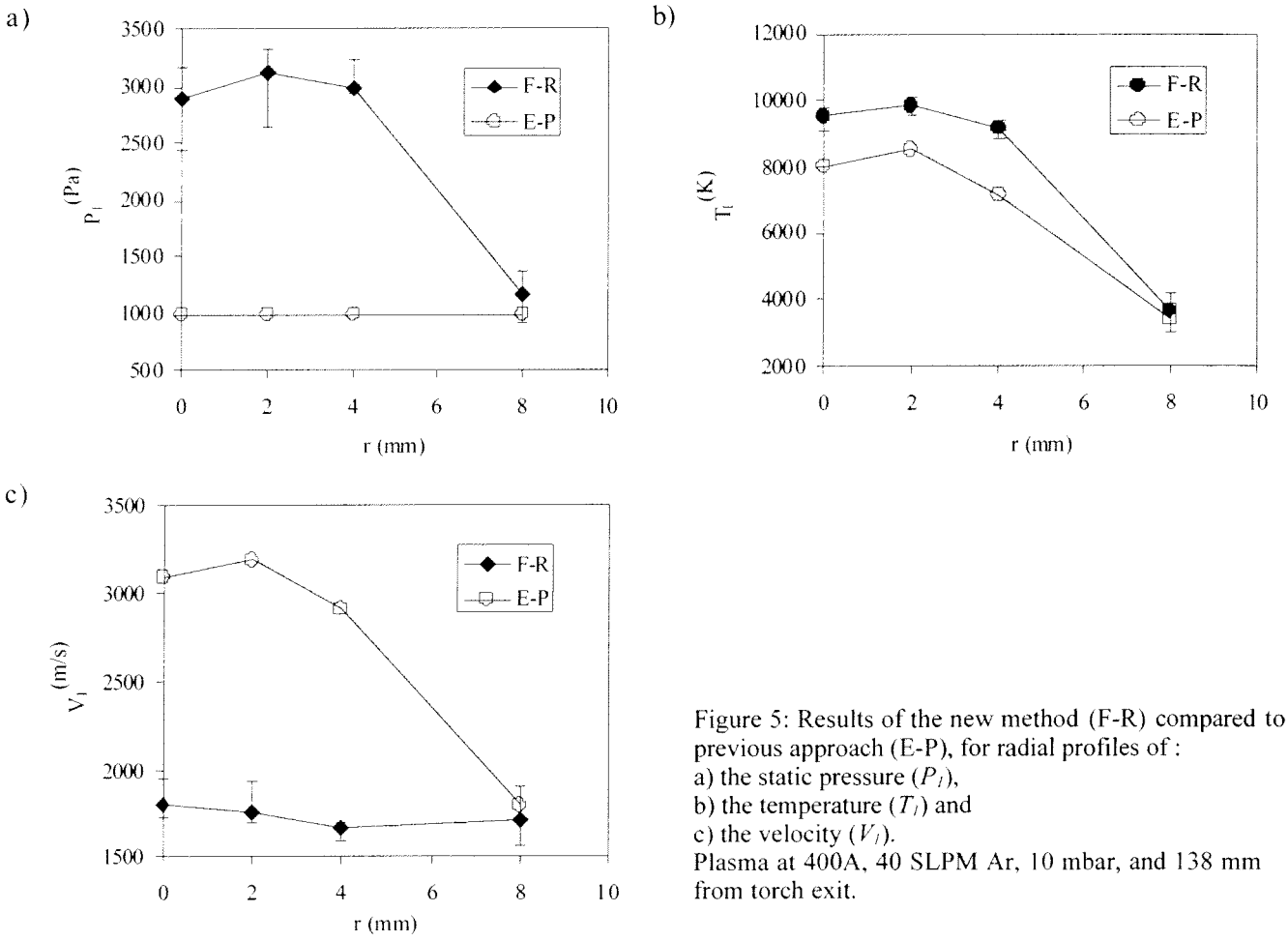

Figure 5: Results of the new method (F-R) compared to previous approach (E-P), for radial profiles of :
a) the static pressure (P_1),
b) the temperature (T_1) and
c) the velocity (V_1).
Plasma at 400A, 40 SLPM Ar, 10 mbar, and 138 mm from torch exit.

In figure 5a, the pressure distribution given by the new approach differs strongly from the one assumed by the classic method (chamber pressure). The new method predicts a higher static pressure than the chamber pressure on the axis, which was foreseen since this axial location is before full expansion (see Fig 3). It is well known that in an expansion zone, expansion waves reduce the jet static pressure radially from a maximum on the axis down to the level of the chamber pressure in the fringe of the jet. This behaviour is captured by the new approach since it predicts a pressure very close to the chamber pressure used in the classic method at the jet fringe where it is close to aerodynamic equilibrium.
The two temperature distributions have the same general trend (Fig 5b), showing a radial temperature drop. An important feature is that both methods predict the same temperature at r = 8mm, where both static pressures are identical. However, the new method gives a higher temperature in the core of the jet.
The two velocity profiles are very different as shown in figure 5c. The new method presents a relatively flat profile compared to the classic method which significantly overestimates the jet velocity on axis (a factor of 1.7 higher). This is due to the fact that the classic method underestimates the core jet static pressure. The flatter profile given by the new approach follows better the free jet boundary layer behaviour predicted by the jet boundary layer theory [13]. Again, the two methods give the same velocity at r = 8mm, due to the aerodynamic equilibrium at this location and provides a validation test case for the new method.

5. Conclusions

The first steps of a new approach have been presented to interpret enthalpy probe measurements performed in supersonic plasma jets which are not in aerodynamic equilibrium. This technique is based on the resolution of the fundamental governing flow equations throughout the NSW induced by the probe and towards stagnation. It uses the second law of Thermodynamics to include non-isentropic effects and relies on the measurement of the post shock static pressure using a specially developed

probe. The advantages of this new approach over previous ones are the less restrictive assumptions and the possibility to include non-LTE effects. In addition, the unknown static pressure of the free jet (usually wrongly approximated by the chamber pressure) is not required as an input, but is obtained as a result of the method.
This new technique has been tested and compared with previous approaches for the case of an under-expanded argon plasma jet produced by a DC plasma torch operated at 10 mbar. The results obtained, in terms of static pressure, temperature and velocity profiles, are consistent with the jet flow phenomenology. Moreover, agreement is found with previous methods at the fringe of the jet where non-aerodynamic equilibrium effects are negligible.
Work is underway to further improve the post-shock static pressure probe developed here, and will allow to extensively characterize the plasma jet flow topology. Inclusion of non-LTE is also foreseen.

Acknowledgments

This work was partially funded by a CTI Swiss Federal Research Projet No. KTI 4403.1KTS. The authors are grateful to Sulzer Metco Switzerland AG for their interest in this work, and for technical support.

References

[1] P. Fauchais and M. Vardelle, "Plasma Spraying: Present and Future", Pure and Appl. Chem., Vol. 66, No. 6, p. 1247-1258, (1994).
[2] M. Loch, and G. Barbezat, "Characteristics and Potential Application of Thermally Sprayed Thin Film Coatings", "Thermal Spray: Surface Engineering via Applied Research", Ed. C. C. Berndt, Pub. ASM International, Material Park, OH, USA, 1141, (2000).
[3] M. Rhamane, G. Soucy, and M. I. Boulos, "Analysis of the enthalpy probe technique for thermal plasma diagnostics", Rev. Sci. Instrum. **66** (6), 3424, (1995).
[4] J.-L. Dorier, M. Gindrat, Ch. Hollenstein, M. Loch, A. Refke, A. Salito, and G. Barbezat, "Plasma jet properties in a new spraying process at low pressure for large are thin film deposition", in Thermal Spray 2001 : New Surfaces for a New Millenium, Pub. ASM International, Materials Park, OH, USA, 2001, p.759-764
[5] B. Jodoin, M. Gindrat, J.L. Dorier, Ch. Hollenstein, M. Loch and G. Barbezat, "Modelling and Diagnostics of a Supersonic DC Plasma Jet Expanding at Low Pressure", Proceedings of the 3rd International Thermal Spray Conference, Essen, Germany, p. 716 – 720, (2002).
[6] M. Hollenstein, M. Rahmane, and M. I. Boulos, "Aerodynamic study of the supersonic induction plasma jet", Proc. of the 14th Int. Symposium on Plasma Chemistry, Prague, Czech Republic, p.257, (1999).
[7] J. R. Fincke, W. D. Swank, S. C. Snider, and D. C. Haggard, "Enthalpy probe performance in compressible thermal plasma jets", Rev. Sci. Instrum. **64** (12), 3585, (1993).
[8] M. Gindrat, J.L. Dorier, Ch. Hollenstein, M. Loch, A. Refke, A. Salito and G. Barbezat, "Effect of Specific Operating Conditions on the Properties of LPPS plasma Jets Expanding at Low Pressure", Proceedings of the 3rd International Thermal Spray Conference, Essen, Germany, p. 459 – 464, (2002).
[9] M. I. Hoffert and H. Lien, "Quasi-One-Dimensional, Nonequilibrium Gas Dynamics of Partially Ionized Two-Temperature Argon", Physics of Fluids, vol. 10 (8), p. 1769-1776, 1967.
[10] A. B. Murphy and C. J. Arundell, "Transport Coefficients of Argon, Nitrogen, Oxygen, Argon-Nitrogen, and Argon-Oxygen Plasmas", Plasma Chemistry and Plasma Processing, vol. 14 (4), p.451-490, 1994.
[11] A.H. Shapiro, "The Dynamics and Thermodynamics of Compressible Fluid Flow Volume I", The Ronald Press Company, New York, 647 p., 1953.
[12] Tekna Plasma Systems Inc., 3535 Boul. Industriel, Sherbrooke, Québec, Canada.
[13] H. Schlichting, "Boundary-Layer Theory 7th Edition", McGraw-Hill Book Company, New York, 817 p., 1987.

Plasma Surface Modified Polystyrene Biochip for Enhanced Biological Coupling

Xin Gao[1], Ch. Hollenstein[2], Manfred Schawaller[3], and Hans-Jörg Mathieu[1,*]
[1] LMCH, Swiss Federal Institute of Technology Lausanne (EPFL),
CH-1015 Lausanne, Switzerland
[2] CRPP, Swiss Federal Institute of Technology Lausanne (EPFL),
CH-1015 Lausanne, Switzerland
[3] DiaMed, Applied Diagnostic Systems AG, 1785 Cressier, Switzerland
*email: hansjoerg.mathieu@EPFLch

Abstract

N_2/H_2 and NH_3/H_2 RF plasmas are used to activate the polystyrene (PS) surface. The capacitively coupled RF plasmas applied for the surface modifications have been characterised by commercial plasma diagnostic methods including ion flux probe, RF power sensor, and mass spectrometer. In particular the ion species and the ion energy have been measured as well as the ion dose impinging onto the polymer surface. The surface modifications are characterized with surface sensitive X-ray Photoelectron Spectroscopy (XPS).

Introduction

Polystyrene (PS) is a popular substrate for disposable ware in medical diagnostic, primarily due to its optical transparency, durability, low cost, and good mouldability.[1] Non-modified polystyrene may cause non-specific adsorption. Therefore it is customary to modify it with hydrophilic polymers.[2] Many polymers such as poly(ethylene glycol) and dextran have been studied for their usefulness in producing pharmacologically active complexes with proteins or drugs. PS surfaces have been successfully modified by high-energy irradiation: γ and UV radiation,[3, 4] plasma treatment[1, 5] and glow discharge plasma.[6]

Plasma surface treatments are potentially very useful for the covalent incorporation into polymer surfaces of extraneous reactive groups suitable for participation in further, conventional chemical reactions at the surface.[7] It is possible to change continuously the chemical composition and properties such as wettability, metal adhesion, dryability, lubricity and biocompatibility of materials surfaces.[8] The plasma modification can be carried out in the presence of specific gases, such as O_2, Ar, He, NH_3, N_2, and H_2. This results in the generation of active species, which can activate and modify the material depending on the nature of the gaseous medium.

The aim of this work is to prepare chemically reactive yet specific PS surfaces for subsequent high-density bio-immobilization such as protein molecules. These modified surfaces are potentially efficient substrates of medical diagnostic tools for use in a proprietary ADS fluorescence reader.[9] The surface modification strategy is shown in Figure 1. In this paper we present the plasma activation and correlated to XPS surface characterization with XPS. Subsequent functionalizations with proteins such as Streptavidin and Neutravidin, and the application study by optical fluorescence measurements will be reported later.

Fig.1 Functionalization (schematic) of a polystyrene chip

Experimental

Polystyrene chips were obtained by injection molding of Polystyrol (BASF). Plasma treatment of PS chips was carried out in a capacitively coupled rf reactor operating at 13.6 MHz. The reactor consisted of two cylindrical electrodes of 13 cm diameter and 4.3 cm apart in a cubic vacuum vessel. The upper electrode and the reactor walls were grounded. The PS chip was placed on the grounded electrode and the system was evacuated to 10^{-6} mbar. The needed gas mixture was introduced into the chamber at a flow rate of 60 sccm and the plasma was operated at a gas pressure of 0.4 mbar at a power of 60 W. The sample exposure time was 3 minutes. The PS chip was directly transferred after exposure for XPS analysis.

For plasma diagnostics only commercial equipment has been used in order to demonstrate that basic plasma diagnostics is now commercially available and to show its necessity for an advanced understanding of the surface modification by plasmas and the industrialisation of the processes. A Scientific System ion flux probe (IFT) has been applied to measure the ion flux on the grounded electrode. A Balzers PPM 422 mass spectrometer system has been used to measure the ion composition and the energy of the impinging ions. Both measuring systems have been incorporated into the grounded electrode. This experimental arrangement permits to measure the characteristics of the ion bombardment at the same place as the treated substrate. Therefore correlations and comparison between plasma parameters and the results from surface analysis can be made.

XPS analysis was performed using an imaging Kratos Axis Ultra X-ray photoelectron spectrometer equipped with a conventional hemispherical analyser. The X-ray source employed was a monochromatized Al Kα (1486.6 eV) source operated at 150 W. Data acquisition was performed under UHV (10^{-9} mbar) conditions. Analysis area was 0.21 mm^2 (300 μm × 700 μm) using a take-off angle of 70° relative to the surface normal. The pass energies were 80 eV and 20 eV for wide scan and high-resolution elemental scans, respectively. The operating software, Vision2, corrects for the transmission function. Charge compensation was performed with a self-compensating device (Kratos patent) using field emitted low energy electrons (0.1 eV) to adjust the main C-C component to 285 eV.[10] The data reduction (atomic concentration, shifting, curve fitting, etc) was performed with CasaXPS Version 2.1.9 software.

Results and Discussion

The electrical asymmetry of the plasma reactor leads to maximum ion energies in the order of 15-20 eV. Under these conditions the ion energy does change only weakly with RF power and other process parameters. Therefore the maximum energy of the bombarding ions for all the cases studied here was below 20 eV (data not shown). However, the energy spectrum depends on the properties of the considered ion. In the case of ions undergoing charge exchange reaction a broad energy spectrum was measured whereas for ions without these reactions the ion energy was peak around the maximum energy.

Table 1 shows the influence of gas mixtures on ion flux and ion doses for various N_2/H_2 and NH_3/H_2 plasmas.

Table 1. Parameters for plasma activations[a]

Prim. Gas / Sec. Gas (% / %)	Ion Flux (mA/cm^2)	Ion dose ($Ions/cm^2$)
100 NH_3 / --	26	2.9E+19
92 NH_3 / 8 H_2	26	3.0E+19
95 N_2 / 5 H_2	87	9.8E+19
90 N_2 / 10 H_2	95	1.1E+20
70 N_2 / 30 H_2	101	1.1E+20

[a] Activation conditions: 60 W, 0.4 mbar, exposure of 3 minutes.

Figure 2 shows the effect of hydrogen dilution on ion compositions when nitrogen is used as a primary gas. In the dilution range from 0-25 % N_2^+, N_2H^+, and H_x^+ are the dominating ions. For higher hydrogen dilutions the measured ion composition is not significantly affected.

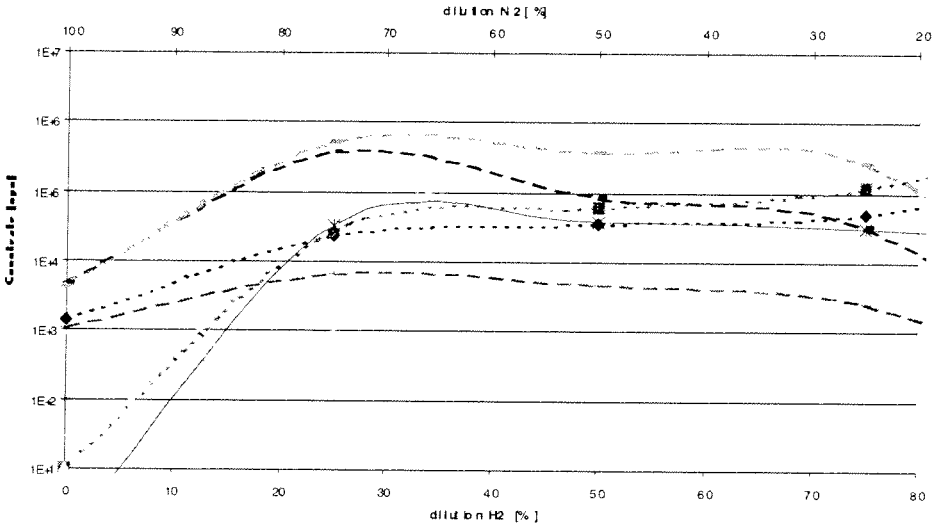

Figure 2. Effect of H_2 admixture on the ion compositions for N_2/H_2 plasmas.

H^+, H_2^+, H_3^+, N^+, N_2^+, N_2H^+, N_3^+, N_4^+.

The effect of hydrogen dilution on ion compositions was also studied for ammonium used as a primary gas. The result is shown in Figure 3. One observes that the admixture of hydrogen doesn't affect the ion composition: NH_x^+ ions are always by far the most abounded ion in these plasmas.

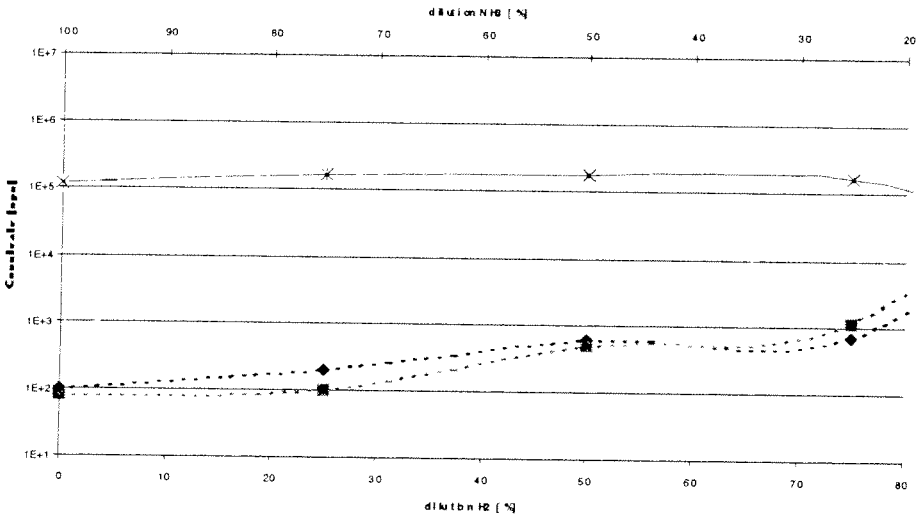

Figure 3. Effect of H_2 admixture on the ion compositions for NH_3 plasma.
H^+, H_2^+; N_3^+, N_4^+.

PS samples are treated with N_2/H_2 (95/5, 90/10, and 70/30 respectively), NH_3/H_2 (92/8) and pure NH_3 plasmas. The efficiency of the plasma activation on PS is checked by nitrogen concentration from XPS analysis. These results are summarized in Table 2. Inspection reveals that hydrogen dilution into a nitrogen plasma has no direct effect on the modification efficiency. According to the results concerning the plasma composition as a function of the hydrogen dilution in N_2 plasma (Figure 2), N_2H^+ ions are the most abundant ion. In the case of hydrogen diluted ammonia plasma NH_x^+ ions are dominating. XPS analysis showed that in these three considered N_2/H_2 plasma cases, similar surface modification efficiencies are observed. Under the present plasma conditions, NH_3 or NH_3/H_2 plasmas are more efficient than N_2/H_2 plasma in providing a nitrogen-amino surface. C1s narrow scan spectrum of PS treated with a NH_3 plasma is shown in Figure 4. Spectra for other samples listed in Table 2 give similar results. Aromatic and aliphatic carbons from PS are observed between 284.7-285.3 eV. As expected, C-N is observed at 286±0.1 eV. The detected oxygen results from the exposure of PS surface to the air when the plasma chamber is opened after the plasma treatment.

Table 2. Nitrogen concentrations of plasma activated PS[a]

Prim. Gas / Sec. Gas (% / %)	at % N
95 N_2 / 5 H_2	11
90 N_2 / 10 H_2	14
70 N_2 / 30 H_2	11
100 NH_3 / --	19
92 NH_3 / 8 H_2	19

[a] Activation conditions: 60 W, 0.4 mbar, exposure of 3 minutes.
error: ± 3 at %

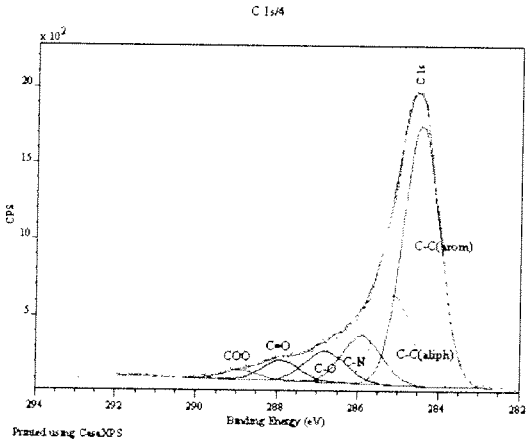

Figure 4. XPS narrow scan spectrum of PS treated with plasma by using pure NH_3. (Take-off angle 70 degree from surface normal)

Although the ion doses of N_2/H_2 plasmas are higher than for the NH_3/H_2 plasma (Table 1), their efficiency to produce nitrogen-containing functional groups at the surface is lower, i.e. that the NH_3 plasma treatment is more effective. Comparing Figure 2 with Table 2 for N_2/H_2 plasmas one notices that the influence of the variation of H_2 is small: although the admixture of H_2 influences strongly the plasma composition in the range from 5-30 %; the nitrogen concentration found at the PS surface remains constant within experimental precision as shown in Table 2. A monolayer of PS contains approximately 10^{15} molecules/cm^2. Compared to the doses values given in Table 2 this means that 10^4-10^5 ions/molecule are needed for nitrogen activation on the PS surface.[11]

Conclusions

The ion energy of the bombarding species is found to be 15-20 eV and the necessary ion density for PS surface activation is 10^4-10^5 ions/molecule per cm^2. H_2 admixture to N_2 or to NH_3 has only small influences on ion composition and nitrogen concentrations at the surface. However a NH_3 plasma is almost two times more efficient than a N_2/H_2 plasma to create active nitrogen-containing sites.

Acknowledgements

The authors would like to acknowledge Nicolas Xanthopoulos for assistance with the XPS analysis. The project was financed on a grant no 6142.MTS of the Commission for Technology and Innovation CTI, Bern Switzerland.

Reference

[1] S. B. Idage, S. Badrinarayanan. Langmuir **14** (1998) 2780-2785.
[2] L. Bromberg, L. Salvati, Jr. Bioconjugate Chem **10** (1999) 678-686.
[3] EC. Onyiriuka. *J Appl Polym Sci.* **47** (1993) 2187.
[4] EC Onyiriuka, LS Hersh, W. Hertl. *J Colloid Interface.* **144** (1991) 98.
[5] D. Keller, K. Schroder, B. Husen, A. Ohl. *Polym Prepr Am Chem Soc Div Polym Chem.* **38** (1997) 1043.
[6] Y. Tamada, Y. Ikada. *Polymer.* **34** (1993) 2208.
[7] T. R. Gengenbach, X. M. Xie, R. C. Chatelier, H. J. Griesser. J. Adhesion Sci. Technol **8** (1994) 305-328.
[8] P. K. Chu, J. Y. Chen, L. P. Wang, N. Huang. Materials Science and Engineering R **36** (2002) 143-206.
[9] patent no. WO 01/14859 A1, EP 1 079 226 A1.
[10] G. Beamson, D. Briggs. *High Resolution XPS of Organic Polymers. The Scienta ESCA300 Database.* John Wiley & Sons Ltd, England, 1992.
[11] X. Gao, Ch. Hollenstein, M. Schawaller, H. J. Mathieu, to be submitted.